5350 *Chem. Mater.* **2010,** *22,* 5350–5357
DOI:10.1021/cm101614p

CHEMISTRY OF MATERIALS
Article

New Route Toward High-Energy-Density Nanocomposites Based on Chain-End Functionalized Ferroelectric Polymers

Junjun Li, Paisan Khanchaitit, Kuo Han, and Qing Wang*

Department of Materials Science and Engineering, The Pennsylvania State University, University Park, Pennsylvania 16802

Received June 9, 2010. Revised Manuscript Received August 5, 2010

The synthesis and characterization of novel ferroelectric polymer based nanocomposites with high energy density is described. The approach includes the preparation of the ferroelectric polymers with phosphonic acid end-groups and subsequent utilization of the reactive terminal groups of the polymer for direct coupling with oxide fillers. The prepared nanocomposites have been carefully characterized by solid-state NMR, DMA, DSC, XRD, and TEM. The formation of covalent coupling between the polymer matrix and ZrO_2 fillers renders the nanocomposites with great stability and uniform filler dispersion. As a result of the intimating coupling, the interfacial interaction regions between the nanoparticles and the polymer matrix, which is responsible for high polarization under the applied fields, have been clearly observed in the dielectric spectra of the nanocomposites. Excellent breakdown strength and substantial enhancement in the energy density have been demonstrated in the nanocomposites. The improvement in the energy storage capability of the nanocomposites has been rationalized on the basis of the changes in polymer microstructures and the rise of the electric displacement induced by the incorporated nanofillers.

Introduction

The development of new materials to store electrical charges is of considerable current interest.[1] Electrical energy storage not only plays an important role in portable electronic devices but also enables future transportation and renewable energy.[2−4] Current energy storage devices include batteries, fuel cells, capacitors, and supercapacitors. Each of these technologies has a different combination of power density and energy density. Among these technologies, capacitors possess the advantage of high power density due to the fast electrical energy storage and discharge capability. With the leaping demand for compact, low-cost, and high efficiency electrical power system, the energy density of capacitor, which is governed by the dielectric materials that separate the opposite static charges, is to be improved further.

Polymers offer an attractive alternative to traditional ceramics as dielectric materials for capacitors because of their great processability, low cost, and lightweight.[5] In addition, polymers generally feature high breakdown strength and a graceful failure mechanism, leading to capacitors with high energy density and great reliability. In particular, poly(vinylidene fluoride) (PVDF)-based ferroelectric polymers exhibit large spontaneous polarization and high dielectric constants because of the presence of highly electronegative fluorine on the polymer chains and the spontaneous alignment of C−F dipoles in the crystalline phases.[6−8] Superior energy density that far exceeds those of conventional dielectric materials, such as biaxally oriented polypropylene (BOPP),[9] has been obtained in a defect-modified PVDF-based copolymer.[10] More recently, the preparation of organic/inorganic hybrid materials composed of ferroelectric polymers and ceramic nanoparticles has also emerged as a promising route to dielectric thin films.[11−16] As the electrostatic energy that can be stored in a dielectric material is related to its dielectric constant and the applied electric field, it is envisaged that the integration of complementary elements such as large dielectric permittivity from ceramic dopants and high breakdown strength from polymer matrix in the

*To whom correspondence should be addressed. E-mail: wang@matse.psu.edu.

(1) *Basic Research Needs for Electrical Energy Storage*; Office of Basic Energy Science, U.S. Department of Energy, Washington, DC, 2007.
(2) Nalwa, H. S., Ed. *Handbook of Low and High Dielectric Constant Materials and Their Applications*; Academic Press: London, 1999.
(3) Whittingham, M. S. *MRS Bull.* **2008**, *33*, 411.
(4) Harden, E.; Ploumen, S.; Fricke, B.; Miller, T.; Snyder, K. *J. Power Sources* **2007**, *168*, 2.
(5) Cao, Y.; Irwin, P. C.; Younsi, K. *IEEE Trans. Dielect. Elect. Insul.* **2004**, *11*, 797.
(6) Lovinger, A. *Science* **1983**, *220*, 1115.
(7) Nalwa, H. S., Ed. *Ferroelectric Polymers*; Marcel Dekker: New York, 1995.
(8) Lu, Y.; Claude, J.; Neese, B.; Zhang, Q. M.; Wang, Q. *J. Am. Chem. Soc.* **2006**, *128*, 8120.
(9) Rabuffi, M.; Picci, G. *IEEE Trans. Plasma Sci.* **2002**, *30*, 1939.
(10) Chu, B.; Zhou, X.; Ren, K.; Neese, B.; Lin, M.; Wang, Q.; Bauer, F.; Zhang, Q. M. *Science* **2006**, *313*, 334.
(11) Chu, B.; Lin, M.; Neese, B.; Zhou, X.; Chen, Q.; Zhang, Q. M. *Appl. Phys. Lett.* **2007**, *91*, 122909.
(12) Dang, Z. M.; Lin, Y. H.; Nan, C. W. *Adv. Mater.* **2003**, *15*, 1625.
(13) Kim, P.; Jones, S. C.; Hotchkiss, P. J.; Haddock, J. N.; Kippelen, B.; Marder, S. R.; Perry, J. W. *Adv. Mater.* **2007**, *19*, 1001.
(14) Arbatti, M.; Shan, X.; Cheng, Z. Y. *Adv. Mater.* **2007**, *19*, 1369.
(15) Li, J.; Claude, J.; Norena-Franco, L. E.; Seok, S. I.; Wang, Q. *Chem. Mater.* **2008**, *20*, 6304.
(16) Li, J.; Seok, S. I.; Chu, B.; Dogan, F.; Zhang, Q. M.; Wang, Q. *Adv. Mater.* **2009**, *21*, 217.

Published on Web 08/23/2010

composites could lead to an enhanced charge storage capacity. However, this approach is strongly handicapped by the difficulty of preparing composites with uniform filler dispersion. This issue becomes severe in the composites based on fluorinated polymers. The unique molecular structures of fluorinated polymers consisting of tightly packed fluorine atoms give rise to low surface energy and interchain forces. As a result, fluorinated polymers generally demix with most organic and inorganic materials, and the dispersion of dopants in the fluorinate polymer matrix always becomes problematic. The agglomeration of the filled ceramic particulates and inevitable formation of voids result in electronic conduction for high loss and dielectric failure at low fields. Although the modification of nanoparticle with a surface layer has been demonstrated to be effective for improving their dispersibility in polymer matrix, these ligands with long (C_6-C_{18}) hydrocarbon chains are usually detrimental to the electrical properties at the applied fields.[17] The alkyl chain with low dielectric permittivity produces local field distortion and enhancement and thus significantly reduces the effective breakdown strength of the composites.[18]

In this study, we report a completely new approach for the preparation of dielectric polymer nanocomposites exhibiting high energy density and excellent breakdown strength. The strategy includes the synthesis of the ferroelectric polymers terminated with phosphonic acids and subsequent utilization of reactive end-groups of the polymer for directly coupling with oxide nanoparticles to yield the covalent-bonded nanocomposites. It is demonstrated herein that covalent assembly of polymer matrix and inorganic filler not only leads to highly dispersed nanofillers without additional surface modification but also provides great stability and offers enhanced interfacial interactions for high polarization responses under the applied fields.

Experimental Section

Materials. 4-(Bromomethyl) benzoic acid (97%), hydrogen peroxide (29−32% w/w aq. solution), and iodotrimethylsilane (97% stab. with copper) were purchased from Alfa Aesar. Triethyl phosphate (98%) was purchased by Aldrich. *N*,*N*′-Dicyclohexylcarbodiimide (DCC, 99.0%) was purchased from Fluka. Zirconium(IV) oxide was obtained from Reade Advanced Materials (Riverside, RI). All the solvents used for the synthesis were ACS grade and used without further purification. Vinylidene fluoride (VDF) and chlorotrifluoroethylene (CTFE) were purchased from SynQuest Laboratory Inc. and purified by the freeze−thaw process prior to use. All manipulations of gas-condense transfer were carried out with rigorous exclusion of oxygen and moisture on a dual-manifold Schlenk line with a 1×10^{-6} Torr high vacuum.

Synthesis of Phosphonate Functional Initiator (1). To a mixture of DCC (0.85 g, 4.13 mmol), dichloromethane (40 mL), and H_2O_2 aqueous solution (1.8 mL, 30%) was added 4-carboxyphenylphosphonate (1.07 g, 3.94 mmol) at −10 °C. The reaction mixture was stirred at −5 °C for 6 h and monitored by thin layer chromatography (TLC). The reaction mixture was filtered and the filter cake was washed with cold dichloromethane several times. The filtrates were combined and the solvent was evaporated. The residue was redissolved in cold dichloromethane and the above step was repeated twice to give a white solid (0.35 g, 35%). ^{1}H NMR (CD_3OD, ppm): δ 8.05 (d, 4H, ArH), 7.58 (d, 4H, ArH), 4.08 (m, 8H), 3.39 (d, 2H), 1.30 (m, 12H). Anal. Calcd For $C_{24}H_{32}O_{10}P$: C, 53.14; H, 5.90. Found: C, 53.11: H, 5.93.

Synthesis of Phosphonic-Acid-Terminated P(VDF-CTFE) Copolymers. The phosphonate functional initiator **1** (0.26 g, 0.48 mmol) and acetonitrile (30 mL) were added in a stainless steel vessel equipped with a magnetic stir bar. The vessel was sealed, submerged in liquid nitrogen, and degassed on a vacuum line. 16.8 g of VDF (0.26 mol) and 1.9 g of CTFE (16.4 mmol) were added to the reactor at liquid nitrogen temperature. The vessel was warmed to ambient temperature and heated for 6 h at 80 °C. After the polymerization, the reactor was cooled down and the residue volatiles were vented. The polymer was subsequently precipitated in methanol and dried in vacuo. 7.0 g of P(VDF-CTFE) was obtained as white solid. ^{1}H NMR (d_6-DMSO, ppm): δ 7.98 (d, ArH), 7.49 (d, ArH), 4.00 (m, 8H), 2.91 ($-CF_2C\underline{H_2}-CF_2CH_2-$, head-to-tail structure), 2.32 ($-CF_2C\underline{H_2}-CH_2CF_2-$, tail-to-tail structure), 1.18 (m, 12H). ^{19}F NMR (d_6-DMSO, ppm): δ −92.4 ($-CH_2CF_2-CH_2C\underline{F_2}-CH_2CF_2-$), −93.7 ($-CFClCH_2-C\underline{F_2}-CH_2-CF-$), −94.8 to −97.1 ($-CF_2CH_2-CH_2C\underline{F_2}$-$CH_2CF_2$-), −108.9 ($-CF_2CH_2C\underline{F_2}CF_2CFCl-$), −114.3 ($-CH_2CF_2-CH_2-C\underline{F_2}-CF_2CH_2-$), −116.1 ($-CH_2CF_2-C\underline{F_2}CH_2-CH_2CF_2-$), −118.2 to −119.9 ($-CH_2CF_2C\underline{F_2}CFClCH_2-$), −120.4 to −121.7 ($-CF_2CF_2C\underline{F}ClCH_2CF_2-$).

The phosphonate-terminated P(VDF-CTFE) (0.50 g) was dissolved in dichloromethane (25 mL) followed by addition of iodotrimethylsilane (0.2 mL, 1.36 mmol). The mixture was stirred at room temperature for 2 h and then evaporated to give a yellow solid. Methanol (20 mL) was added and the suspension was stirred for 1.5 h. The product (0.41 g) was collected by filtration. ^{1}H NMR (d_6-DMSO, ppm): δ 7.91 (d, ArH), 7.43 (d, ArH), 2.89 ($-CF_2C\underline{H_2}-CF_2CH_2-$, head-to-tail structure), 2.24 ($-CF_2C\underline{H_2}-CH_2CF_2-$, tail-to-tail structure).

Preparation of the Nanocomposite Films. The phosphonic acid terminated P(VDF-CTFE) was dissolved in anhydrous *N*, *N*-dimethylformamide (DMF) and stirred for 12 h at room temperature to make a transparent solution. ZrO_2 nanoparticles were dried in vacuo at 120 °C for 12 h to remove the surface-bound water, and then dispersed in DMF (4 mg/mL). This dispersion was subjected to sonication using Vibra-Cell high intensity ultrasonic processor (VC-505) for 30 min with vigorous stirring. The polymer solution was added into ZrO_2 suspension slowly and the mixture was stirred at ambient temperature for 12 h. The mixture underwent a second sonication for 30 min before it was poured onto clean glass slide (7.5 × 5.0 cm) at 50 °C. After being dried at 70 °C under atmospheric pressure for 12 h, the film was transferred into a vacuum oven and baked at 90 °C for 4 h, 120 °C for 4 h, and 150 °C for 24 h in order to remove the remaining trace of solvent and enhance the Zr−OH/P−OH condensation. The resulting film was cooled down to room temperature, immersed in deionized water for 2 h, and peeled off from glass slide. After being dried in vacuo at 60 °C for 12 h, the sample films were placed between two Teflon sheets and melt pressed at 150 °C under 600 psi for 20 min. The free-standing films were obtained after being cooled naturally to room temperature in melt-pressing instrument. The typical thickness of the films is around 20−30 μm.

(17) Cho, S. D.; Paik, K. W. *Proceedings of the 51st IEEE Electronic Components and Technology Conference*; May 29−June 1, 2001; IEEE: Piscataway, NJ, 2001; p 1418.
(18) Li, J. Y.; Zhang, L.; Ducharme, S. *Appl. Phys. Lett.* **2007**, *90*, 132901.

Scheme 1. Synthesis of the Functional Initiator and the Phosphonic-Acid-Terminated P(VDF-CTFE)

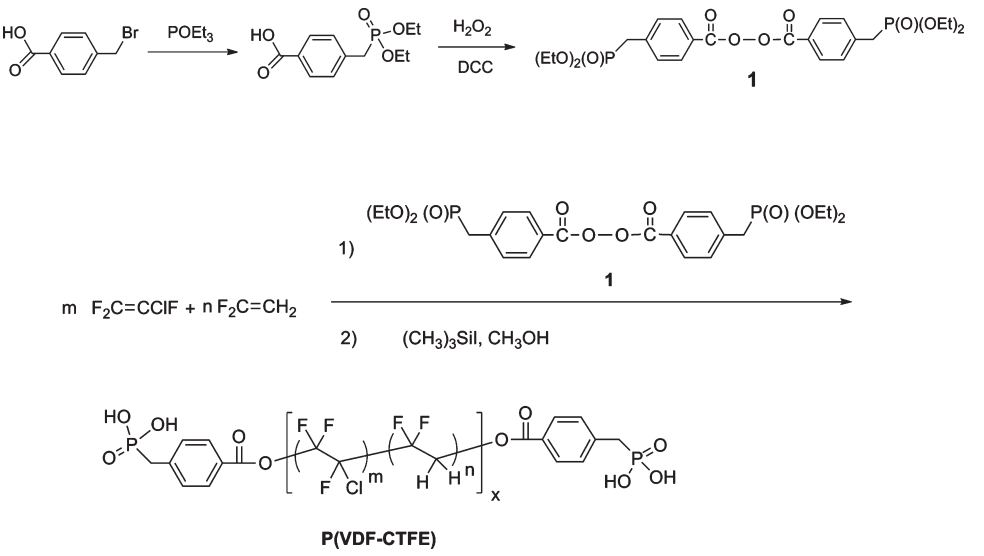

Characterization. ^{1}H and ^{19}F NMR spectra were recorded on Bruker AM-300 spectrometer at room temperature using tetramethylsilane (TMS) and CF_3Cl as internal references, respectively. Direct-polarization magic angle spinning (MAS) ^{31}P solid-state NMR spectra of the phosphonic acid terminated P(VDF-CTFE) and the composites film were acquired on Chemagnetics-Varian Infinity 500 spectrometer with a ^{31}P transmitter frequency of 202.36 MHz. ^{31}P signals were externally referenced to 85% H_3PO_4. Direct polarization techniques with continuous wave (cw) proton decoupling were used throughout. The decoupling field was on the order of 40 kHz. A ^{31}P excitation pulse width of 4 microseconds was used. Spinning frequency was set to 6.5 kHz. The pulse delay was 5 s and the number of scans was 13844 for P(VDF-CTFE) and 2288 for the composites. Molecular weights and polydispersity of the phosphonate terminated P(VDF-CTFE) were determined in a DMF mobile phase at a flow rate of 1.0 mL/min using gel permeation chromatography (GPC). The instrument is Viscotek Model 302 triple detection system equipped with refractive index, light scattering and viscometer detectors, and the columns were Viscogel I-Series for intermediate polar polymers. The thermal transition data were obtained by a TA Instrument Q100 differential scanning calorimeter (DSC) and a TA Instrument model Q50 (thermogravimetric analysis, TGA) at a heating rate of 10 °C/min under N_2. Dynamic mechanical analysis measurements were performed on TA Instruments DMA Q800 from −60 to 80 °C at the ramp rate of 3 °C/min in tensile mode. Wide-angle X-ray diffraction (WAXD) measurements were conducted using a Scintag diffractometer with Cu Kα radiation (wavelength λ = 0.154 nm). Transmission scanning microscopy (TEM) experiments were performed using JEOL JEM-1200 EX II TEM equipment and the sample was made by cryo-microtome.

To examine the dielectric properties of the composites, we sputtered circular gold electrodes with diameter of 2.6 mm and a typical thickness of 30 nm on both sides of the films for the electric measurements. Dielectric constant (ε) and loss (tan δ) at room temperature were measured using an Agilent LCR meter (E4980A) from 100 Hz to 2 MHz. Dielectric relaxation spectroscopy (DRS) of the polymer and nanocomposites has been investigated using a LCR meter equipped with a temperature chamber at 1 V bias.[19] The polarization-electric field (*P-E*) loops were recorded using a modified Sawyer−Tower circuit at the electric field up to 270 MV/m.[10] The energy density of samples was determined from the integration of unipolar *P*−*E* loops.

Results and Discussion

Chain-End Functionalized Polymers. The incorporation of functional groups into the ferroelectric fluorinated polymers for covalent-bonded assemblies can be accomplished via copolymerization with comonomers containing pendant functional groups.[20] However, the introduced side chains usually impair crystallization of the polymers and greatly alter the polymer chain conformation and solid-state structure. The dramatic reduction in the crystallinity of the polymers would result in a decrease or even a total loss of the associated ferroelectricity and polarization.[6] Therefore, telechelic structures in which functional groups are introduced at the polymer chain ends are highly desirable herein.[21] This chain-end functionalization approach would keep the main chain structure of the polymers intact and thus preserve unique electrical properties of the ferroelectric polymers to a large degree in the assemblies.

To synthesize telechelic structures of the ferroelectric polymers, we developed a polymerization method based on the functional benzoyl peroxide for fluorinated alkene.[22] As shown in Scheme 1, telechelic poly(vinylidene fluoride-*co*-chlorotrifluoroethylene), P(VDF-CTFE) (91/9 mol %), containing phosphonate terminal groups was prepared using a functional benzoyl peroxide (**1**) as the initiator. Compound **1** was obtained by the condensation of

(19) Lu, Y.; Claude, J.; Norena-Franco, L. E.; Wang, Q. *J. Phys. Chem. B* **2008**, *112*, 10411.
(20) Ameduri, B.; Boutevin, B.; Kostov, G. *Prog. Polym. Sci.* **2001**, *26*, 195.
(21) Goethals, E. J., Ed. *Telechelic Polymers: Synthesis and Applications*; CRC Press: Boca Raton, FL, 1989.
(22) Li, K.; Liang, S.; Lu, Y.; Wang, Q. *Macromolecules* **2007**, *40*, 4121.

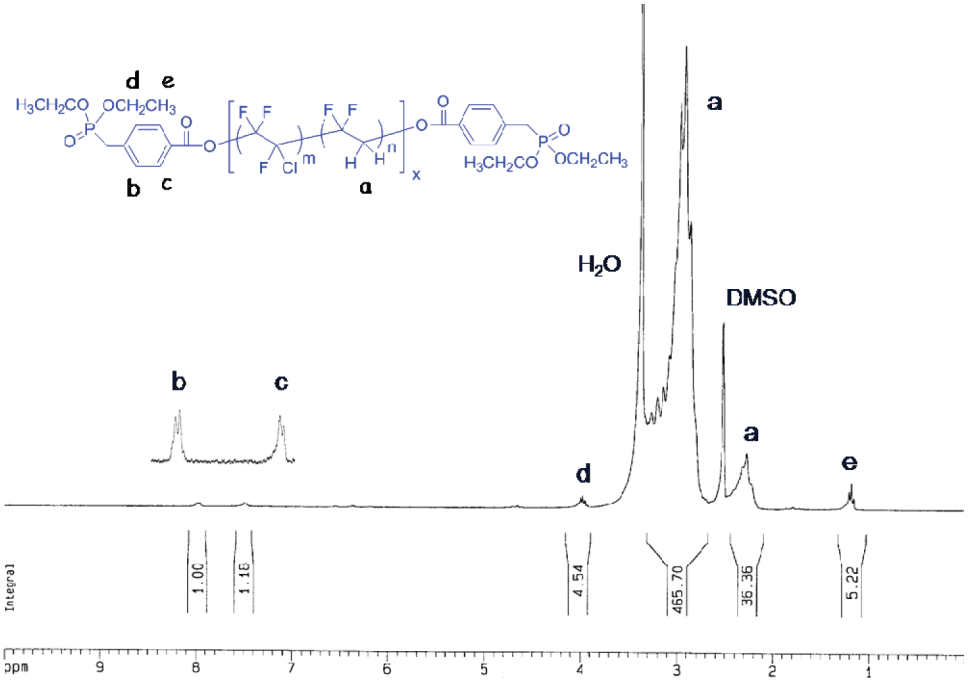

Figure 1. ^{1}H NMR spectrum of P(VDF-CTFE) with phosphate terminal groups.

4-carboxyphenylphosphonate in the presence of H_2O_2 and DCC. As the termination in radical polymerization of fluorinated alkenes proceeds exclusively through the radical coupling,[23,24] the functional groups in the initiator are expected to be transferred to the polymer chain ends after polymerization. Indeed, as shown in Figure 1, the ^{1}H NMR spectrum of P(VDF-CTFE) displays the distinctive signals at 1.18 and 4.00 ppm corresponding to the phosphonate groups and the resonances at 7.49 and 7.98 pm assigned to the aromatic protons. The characteristic multiplet centered at 2.9 ppm in the ^{1}H NMR spectrum is assigned to the methylene groups of $-CF_2CH_2-CF_2CH_2-CF_2CH_2-$ resulting from the normal head-to-tail (H−T) VDF addition. This agrees well with the signals at −93.0 and −95.2 ppm shown in the ^{19}F NMR spectrum, which are attributed to the difluoromethylene groups in $-CH_2CF_2-CH_2CF_2-CH_2CF_2-$ and $-CH_2CF_2-CF_2CH_2-CH_2CF_2-CH_2CF_2-$ sequences, respectively. Additionally, the ^{19}F NMR spectrum exhibits the expected multiplets centered at −114.3 and −116.1 ppm, corresponding to the head-to-head (H−H) VDF sequence in the polymer chain. The mole fraction of H−T sequence assessed from the integrals of the characteristic peaks was found to be around 95%.

The ^{1}H and ^{19}F NMR analyses revealed a number-average molecular weight (M_n) of 26200 g/mol for the P(VDF-CTFE), whereas the triple-detection GPC measurements in DMF gave a M_n of 28 000 g/mol with a polydispersity index of 1.3. The average degree of functionality, f, was calculated by comparison of the number average molecular weights from NMR and GPC measurements according to the following equation[25]

$$\frac{x(\text{repeating unit from GPC})}{\text{number of protons at two end groups}} = \frac{(\text{sum of } CH_2\text{integrals})/2}{(\text{integral of protons from end groups})/f} \quad (1)$$

It was determined that ~95% of the polymer chains carry two functional end-groups and the average degree of functionality is around 1.9, close to the theoretical value of 2. The phosphonate end groups were subsequently transformed into phosphonic acids using iodotrimethylsilane, as verified by complete disappearance of the ethyl proton peaks in the ^{1}H NMR spectrum.

Nanocomposite Preparation and Characterization. Thin films of the nanocomposites were fabricated by casting the solution of the phosphonic acid terminated P(VDF-CTFE) and ZrO_2 (average size: ~10 × 40 nm) in DMF on glass substrate and then annealed and hot-pressed. ZrO_2 nanoparticle was chosen as the filler because its dielectric permittivity of 21 is comparable to that of the P(VDF-CTFE) matrix (i.e., 11@ 1 kHz). This is anticipated to benefit the breakdown strength by reducing the contrasts in the permittivity and field between the nanofillers and the polymer matrix and creating dielectric homogeneity in the composites.[18] The interaction between the phosphonic acid end-groups of P(VDF-CTFE) and ZrO_2 was probed by the cross-polarization MAS ^{31}P solid-state NMR spectroscopy. As shown in Figure 2, the ^{31}P NMR signal shifts from 45 ppm in the phosphonic acid terminated P(VDF-CTFE) to 28 ppm in the nanocomposites containing 4.8 wt % ZrO_2. This significant upfield

(23) Timmerman, R. J. *Appl. Polym. Sci.* **1962**, *6*, 456.
(24) Guiot, J.; Ameduri, B.; Boutevin, B. *Macromolecules* **2002**, *35*, 8694.
(25) Edelmann, D.; Ritter, H. *Makromol. Chem.* **1993**, *194*, 2375.

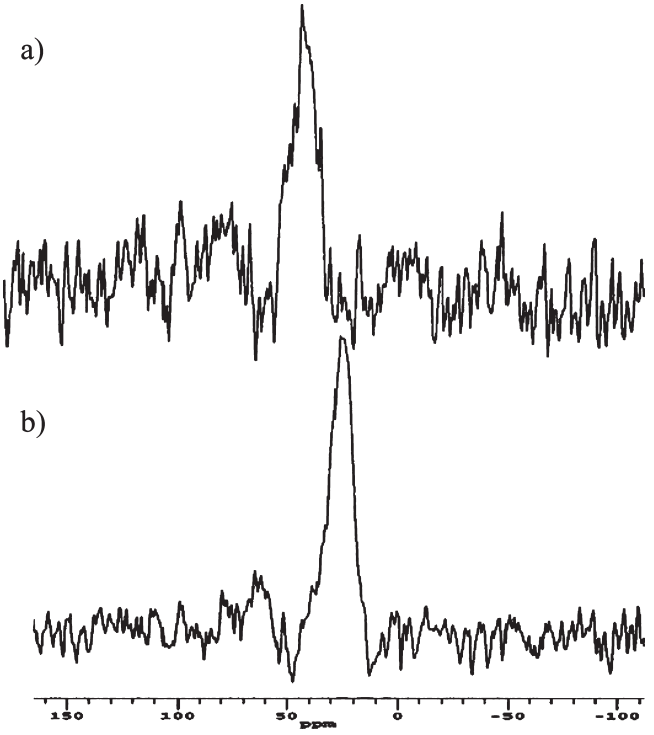

Figure 2. ^{31}P solid-state NMR spectra of (a) phosphonic-acid-terminated P(VDF-CTFE); (b) P(VDF-CTFE)−4.8 wt % ZrO_2 nanocomposites.

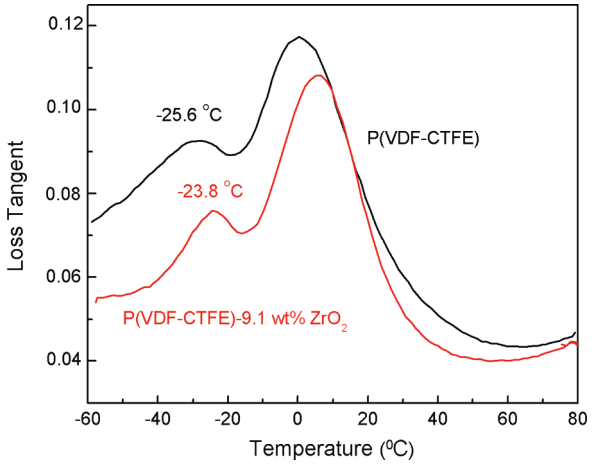

Figure 3. Temperature dependence of the mechanical loss (at 2 Hz) of P(VDF-CTFE) and the nanocomposite.

shift is ascribed to bidentate binding mode of terminal phosphonic acids on ZrO_2.[26] The coupling of the polymer with the nanoparticles was further substantiated by the increase of the glass transition temperature from −25.6 °C in P(VDF-CTFE) to −23.8 °C in the nanocomposites as shown in dynamic mechanical analysis depicted in Figure 3. Consequently, the formation of covalent bonds[27] offers great stability of the composites. For instance, the composite thin films remain intact upon heating at 200 °C, while the neat polymer melts at ∼120 °C. The graft density of the

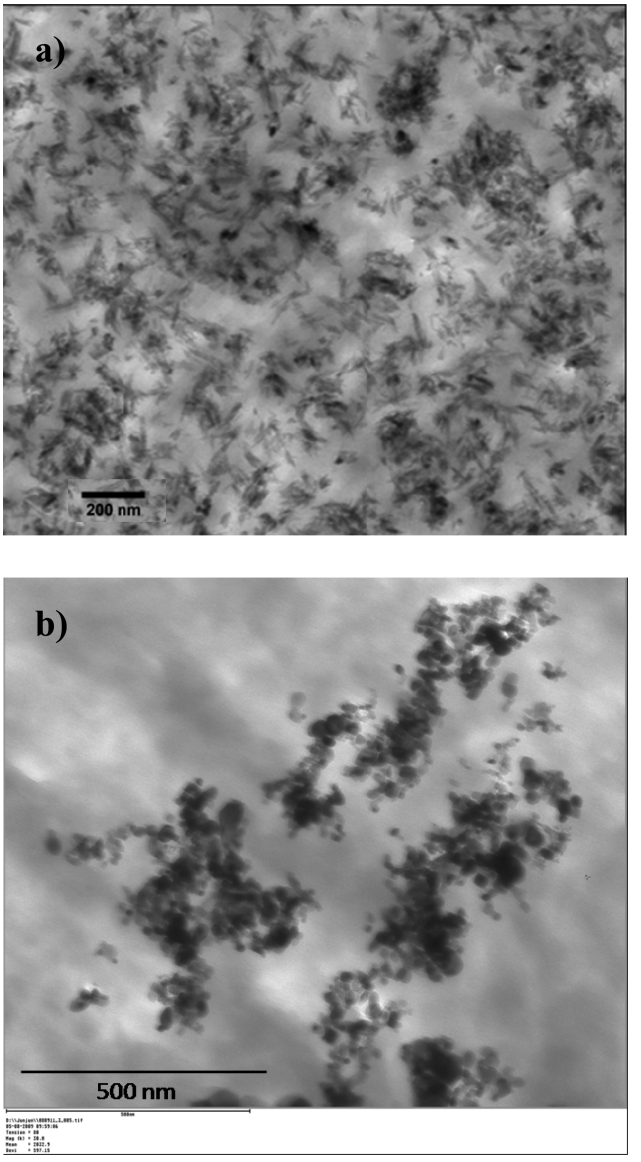

Figure 4. TEM image of (a) the covalent-bonded P(VDF-CTFE) and (b) pristine P(VDF-CTFE) composites with 12 wt % ZrO_2.

polymer on the ZrO_2 nanoparticle surface was estimated by TGA analysis according to eq 2 [28]

$$\text{graft density} = \{[(W-(100-W)100-W_{\text{particle}}]/MS100\}\times 10^6 \quad (2)$$

where W is the weight loss between 60 and 730 °C corresponding to decomposition of the immobilized polymer chains, M is the molecular weight of the grafted polymer, and S and W_{particle} are respectively the specific surface and the weight loss of the particle determined before grafting. S was measured using BET (Brunauer−Emmett−Teller)-adsorption isotherms method and found to be ∼26.3 m^2/g. The calculation gave a grafting density of ∼0.4 chain/nm^2.

The TEM images illustrated in Figure 4a corroborate that ZrO_2 nanoparticles are randomly dispersed in the

(26) Gao, W.; Dickinson, L.; Grozinger, C.; Morin, F. G.; Reven, L. *Langmuir* **1996**, *12*, 6249.
(27) Mutin, P. H.; Guerrero, G.; Vioux, A. *J. Mater. Chem.* **2005**, *15*, 3761.
(28) Bartholome, C.; Beyou, E.; Bourgeat-Lami, E.; Chaumont, P.; Zydowicz, N. *Macromolecules* **2003**, *36*, 7946.

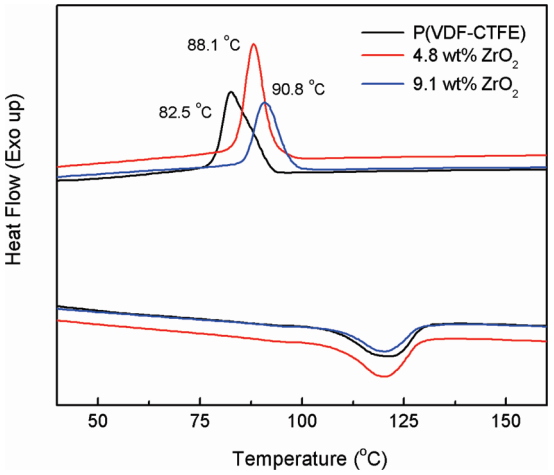

Figure 5. DSC profiles of P(VDF-CTFE) and the nanocomposites.

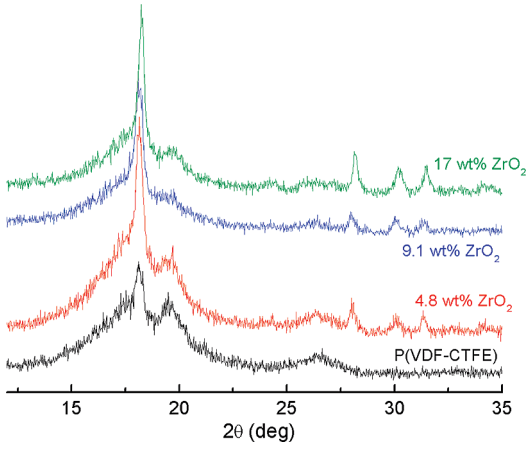

Figure 6. WXRD patterns of P(VDF-CTFE) and nanocomposites.

chain-end functionalized P(VDF-CTFE) matrix without noticeable signs of aggregation. On the other hand, agglomeration of ZrO_2 filler in the polymer matrix has been clearly seen in the composites of unfunctionalized P(VDF-CTFE) and ZrO_2 (Figure 4b), which was prepared by mixing of pristine P(VDF-CTFE) and ZrO_2 for the purpose of comparison.

The effect of ZrO_2 nanoparticles on the microstructure of the polymer matrix has been examined by DSC and WAXD. The DSC profiles of the polymers and the nanocomposites recorded during heating and cooling scans are displayed in Figure 5. It was found that the introduction of the nanoparticles into the polymer raises the crystallization temperatures, from 82 °C for P(VDF-CTFE) to 91 °C for the nanocomposite containing 9.1 wt % ZrO_2. Consistent with the change in the crystallization temperatures, the enthalpy of melting in the nanocomposites increases progressively from 15.9 J/g from P(VDF-CTFE) to 19.8 J/g for the composite with 9.1 wt % ZrO_2 nanoparticles, which corresponds to a change of the degree of crystallinity from 18.3% for the neat polymer to 22.8% for the composites. No appreciable change in thermal properties was observed in the nanocomposites when the ZrO_2 content is increased above 9.1 wt %. As shown in Figure 6, the WAXD patterns of the nanocomposites

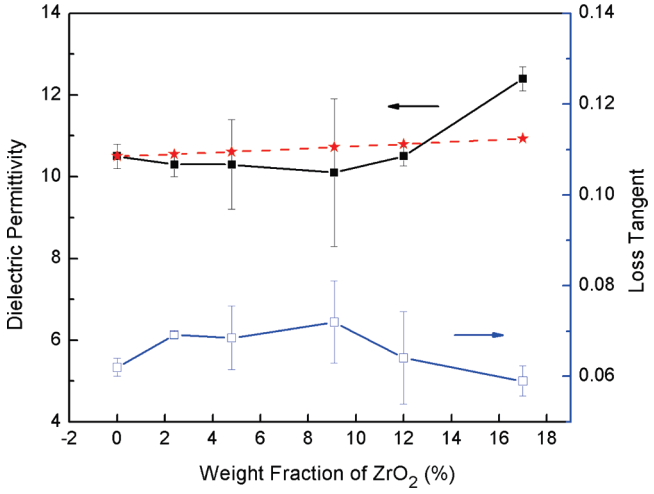

Figure 7. Dielectric permittivity and loss tangent of P(VDF-CTFE) and the nanocomposites measured at 1 kHz and room temperature. Stars are the effective dielectric permittivity of the composites calculated from the Lichtenecker law.

display a main peak at a 2θ angle of 18.1° related to the (020) diffraction from the crystalline α phase in the polymer.[29] The size of crystalline domain was calculated by Scherrer's formula

$$t = \lambda / B\cos\theta \qquad (3)$$

where t is the crystallite size, λ is the wavelength of X-ray (1.54 Å), B is the normalized full width at half-maximum (fwhm) of diffraction peaks from the JADE software, and θ is the diffraction angle. With increasing nanoparticle content, this peak becomes sharper, indicating that the crystallite size successively increases from ~5 nm in the polymer to ~20 nm in the nanocomposites containing 9.1 wt % ZrO_2. The diffraction peaks at 28.0, 30.0, and 31.4 are assigned to the monoclinic phase of ZrO_2 nanocrystals, whose intensities are obviously pronounced as the concentration of the nanoparticle increases. This result strongly suggests that the nanoparticles act as nucleating agents to improve the crystallinity of the polymer, which is in accordance with the variation of the crystallization temperature and the enthalpy of melting and also consistent with other reports.[30,31]

Dielectric Properties. Figure 7 shows the dielectric permittivity and loss tangent measured using a multifrequency LCR meter at 1 V bias. Because P(VDF-CTFE) and ZrO_2 have comparable dielectric permittivities, unsurprisingly, there is no drastic change of the dielectric permittivities of the nanocomposites until the content of ZrO_2 reaches 17 wt % where improved dielectric permittivity was observed. The error bar in the dielectric permittivity is ascribed to the variation in the film thickness. The effective dielectric permittivity of the composites was calculated according to the Lichtenecker

(29) Lovinger, A. J.; Davis, G. T.; Furukawa, T.; Broadhurst, M. G. *Macromolecules* **1982**, *15*, 323.
(30) Levi, N.; Czerw, R.; Xing, P.; Lyer, P.; Carrol, D. *Nano Lett.* **2004**, *4*, 1267.
(31) Shah, D.; Maiti, P.; Gunn, E.; Schmidt, D. F.; Jiang, D. D.; Batt, C. A.; Giannelis, E. P. *Adv. Mater.* **2004**, *16*, 1173.

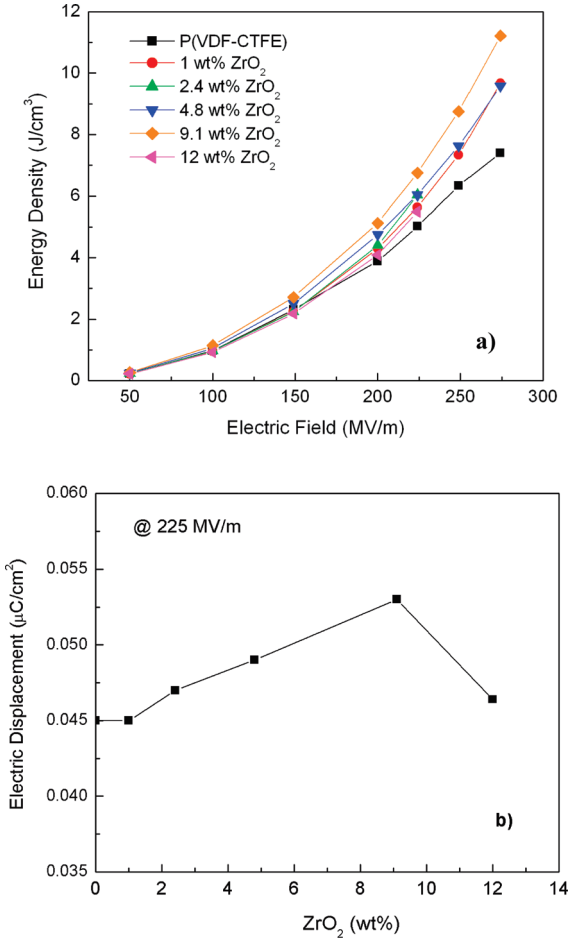

Figure 8. (a)Stored energy density of the polymer and the nanocomposites as a function of the applied field. (b) Dependence of maximum electric displacement on the ZrO_2 content in the nanocomposites measured at 225 MV/m.

logarithmic mixing rule[32]

$$\log \varepsilon = y_1 \log \varepsilon_1 + y_2 \log \varepsilon_2 \qquad (4)$$

where y_1 is the volume fraction of inorganic filler with a permittivity of ε_1, and y_2 is the volume fraction of polymer matrix with a permittivity of ε_2. As illustrated in Figure 7, the calculated results confirm the steady permittivity of the composites at low contents of ZrO_2, but the model becomes inaccurate at high concentrations of the nanoparticle (> 16 wt %) where the predicted values are lower than those measured. The dielectric loss tangent of the composites is dominated by the polymer matrix and shows little dependence on the filler content, which further implies homogeneous dispersion of ZrO_2 in the polymer matrix.

Interestingly, it was found that the incorporation of ZrO_2 nanoparticles into the polymers greatly increases the energy density of the materials at high fields, which is in marked contrast to the weak-field dielectric properties. As summarized in Figure 8a, the energy density of the composite increase with the content of ZrO_2 nanoparticles and reaches a maximum at around 9.1 wt % ZrO_2. For the composites with 9.1 wt % ZrO_2, the energy density is 11.2 J/cm^3 at 270 MV/m, representing a ~60% increase in comparison to the polymer matrix at the same field. This value is significant and exceeds those reported for the conventional polymer-ceramic composite dielectrics.[33−35] Of particular note is that the measured breakdown strength of over 270 MV/m is comparable to that of the polymer matrix and considerably higher than the conventional dielectric polymer nanocomposites. This result is mostly likely due to the balanced dielectric permittivities of two constituents and diminished defects in the nanocomposites as a result of the intimate coupling of the filler and the matrix. The enhanced energy densities can be attributed to the increase in the crystallinity of the polymer induced by the existence of the nanoparticles as shown in our DSC and WAXD studies. Since the crystallization region in the ferroelectric polymers is responsible for polarization,[6] an improved crystallinity gives rise to a high polarizability and permittivity at high fields.

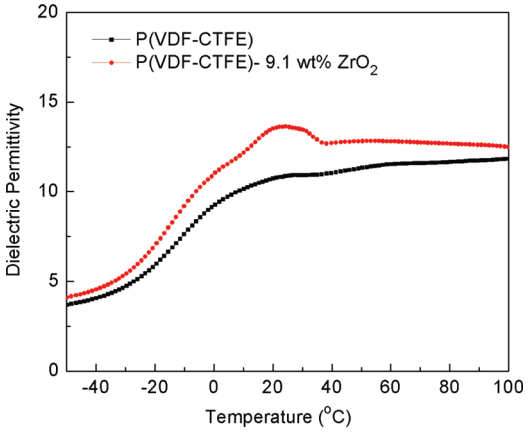

Figure 9. Temperature-dependence of the dielectric permittivity of the polymer and covalent-bonded nanocomposites measured at 10 kHz.

Additionally, it has been proposed that the interfacial coupling effect plays an important role in determining the energy density at high fields in dielectric nanocomposites.[36,37] The large interface area in the nanocomposites would produce the Maxwell−Wagner−Sillars (MWS) interfacial polarization and lead to an "interaction zone" with the Gouy−Chapman diffuse layer, thereby greatly affecting the polarization and electrical displacement of the polymer matrix near the fillers.[38] The presence of the interfacial interaction region in the nanocomposites has been clearly evidenced in the temperature dependence of dielectric permittivity shown in Figure 9. Compared to the base polymer, the nanocomposite exhibits an additional dielectric anomaly appearing at higher temperature,

(32) Rao, Y.; Qu, J. M.; Marinis, T.; Wong, C. P. *IEEE Trans. Compon., Packag. Technol.* **2000**, *23*, 680.
(33) Tanaka, T.; Montanari, G. C.; Mülhaupt, R. *IEEE Trans. Dielect. Elect. Insul.* **2004**, *11*, 763.
(34) Ma, D.; Hugener, T. A.; Siegel, R. W.; Christerson, A.; Mårtensson, E.; Önneby, C.; Schadler, L. S. *Nanotechnology* **2005**, *6*, 724.
(35) Gilbert, L. J.; Schuman, T. P.; Dogan, F. *Ceram. Trans.* **2006**, *179*, 17.
(36) Lewis, T. J. *J. Phys. D: Appl. Phys.* **2005**, *38*, 202.
(37) Tanaka, T.; Kozako, M.; Fuse, N.; Ohki, Y. *IEEE Trans. Dielect. Elect. Insul.* **2005**, *12*, 669.
(38) Nelson, J. K.; Fothergill, J. C. *Nanotechnology* **2004**, *15*, 586.

which can be ascribed to the dipolar glass freezing transition from the polymer chains bonded to the nanoparticles.[19] In accordance with the change in glass transition temperature, the existence of covalent bonds restricts the chain mobility of the polymer segment around the nanoparticles and thus enhances the activation energy of the transition. The dielectric spectra of pristine P(VDF-CTFE) and ZrO_2 nanocomposites were also measured for comparison, in which the peaks arising from the interfacial areas are almost unnoticeable. This is probably due to poor affinity between the hydrophilic fillers and the hydrophobic fluorinated polymer matrix.[36] The rise of the electrical displacement due to the incorporation of the ZrO_2 nanoparticles shown in Figure 8b is thus believed to account for the improved energy densities observed in the covalent-bonded nanocomposite. The energy density of the nanocomposites was found to decrease when the nanoparticle loading is higher than 9.1 wt %. Although a detailed mechanism for this change in energy density remains to be established, it possibly arises from the increased conduction loss and/or reduction of the interfacial effect because of coalescing of the interfacial area at high filler concentrations.[16]

Conclusions

In summary, we have demonstrated a unique route, using chain-end functionalization of the ferroelectric polymer, to prepare covalent-bonded polymer nanocomposites with uniform nanoparticle dispersion. The nanocomposites exhibit remarkable dielectric strengths without the usual penalty of sacrificing electric strength and greatly improved energy densities than the matrix. Furthermore, the prepared nanocomposites have been shown excellent stability. The films have been tested repeatedly over ~1.5 years under ambient conditions and deterioration of the breakdown strength and the energy density has not been observed. This result suggests an important improvement over what has been reported in the past with the conventional dielectric polymer nanocomposites. As phosphonic acid shows an excellent affinity toward a variety of oxides such as TiO_2, $BaTiO_3$, and $SrTiO_3$,[26] we expect that this strategy can be generalized to the preparation of diverse nanocomposites containing electroactive polymers and nanoparticles with synergic properties for electrical energy storage applications.

Acknowledgment. This work was supported by the National Science Foundation and the Office of Naval Research.